Volume 15
Number 7
7 April 2025
Pages 2051–2396

# Catalysis Science & Technology

rsc.li/catalysis

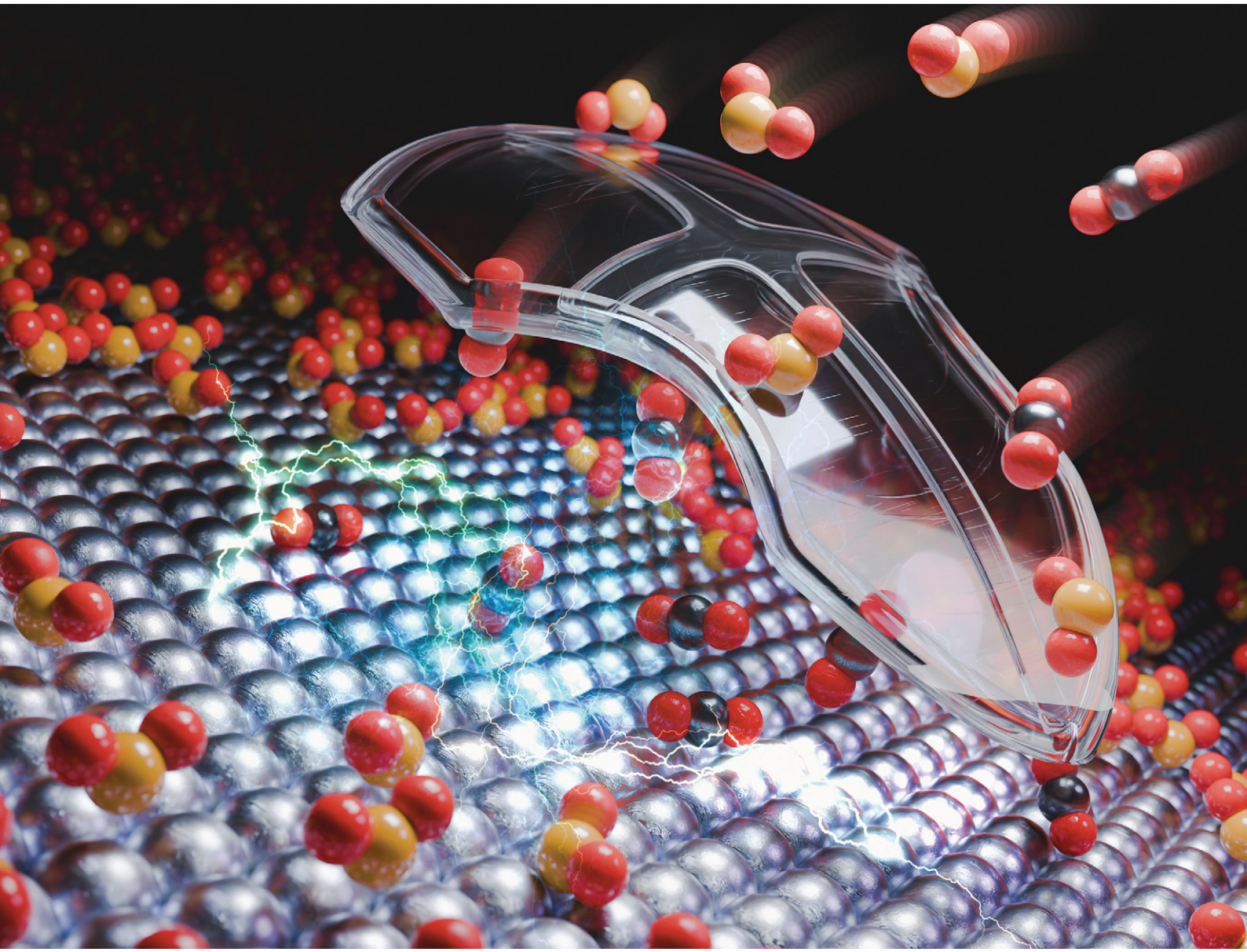

ISSN 2044-4761

ROYAL SOCIETY OF CHEMISTRY

**PAPER**

Ming Li, J. Ruud van Ommen *et al.*

The effects of $SO_2$ impurities on $CO_2$ electroreduction on bare silver and $SiO_2$ coated silver in different cell geometries

Catalysis Science & Technology

ROYAL SOCIETY OF CHEMISTRY

PAPER

View Article Online
View Journal | View Issue



Cite this: *Catal. Sci. Technol.*, 2025, **15**, 2148

# The effects of $SO_2$ impurities on $CO_2$ electroreduction on bare silver and $SiO_2$ coated silver in different cell geometries†

Ming Li, *[a] Shilong Fu,[b] Ruud Kortlever [b] and J. Ruud van Ommen *[a]

Electrochemical $CO_2$ reduction presents an opportunity to transform waste flue gas with water and renewable electricity into chemicals or fuels. However, the energy-intensive nature of purification of flue gas underscores the appeal of directly utilizing the flue gas streams containing impurities. In this study, we investigate the impact of $SO_2$ impurities on $CO_2$ electroreduction in two electrochemical cell geometries: an H-cell and a membrane electrode assembly (MEA) cell. We observe distinctly different behavior of the Ag on carbon black (Ag/CB) catalyst under $SO_2$ impurities in the H-cell compared to the MEA cell, where $SO_2$ impurities exhibit a more pronounced effect on Ag/CB catalysts in the H-cell than in the MEA cell. This difference is attributed to the higher solubility of $SO_2$ in the electrolyte compared to $CO_2$, resulting in an accumulation effect and causing differences in the $SO_2$ concentration near the electrode between the H-cell and the MEA system. By depositing a very thin $SiO_2$ coating on the outermost surface of the Ag/CB catalyst using atomic layer deposition (ALD), the impact of $SO_2$ on the catalyst's selectivity is diminished. This is attributed to the permeability difference between $CO_2$ and $SO_2$ through the $SiO_2$ coatings and results in a local $SO_2$ concentration difference between samples with and without $SiO_2$ coatings.

Received 8th October 2024,
Accepted 7th January 2025

DOI: 10.1039/d4cy01196a

rsc.li/catalysis



## Introduction

With the ongoing rise in global $CO_2$ emissions, there is an urgent need to develop sustainable technologies for capturing and utilizing $CO_2$. The electrochemical reduction of $CO_2$ offers an appealing method for transforming surplus $CO_2$, along with water and renewable electricity, into bulk chemicals that can be directly used in the process industry or as fuels, as depicted in Fig. 1. The electrochemical reduction of $CO_2$ to CO is particularly intriguing as this is a two-electron reduction product, resulting in significant yields from each mole of electron transfer.[1] Silver (Ag) is one of the best catalysts for the electroreduction of $CO_2$ to CO because of its high selectivity for CO during $CO_2$ reduction and its high stability over prolonged periods of operation.[2–5] However, the Ag catalyst is susceptible to poisoning and subsequent loss of activity during the reaction due to the presence of impurities in the reactants.[6–9] And the $CO_2$ streams from industry often contain a variety of pollutants, and the $CO_2$ concentration typically is relatively low, compared to the close to 100% for carbon capture from the air or from seawater (ranging from 3 to 45% from power plants and steel manufacturing factories).[10] The anticipated costs of capturing $CO_2$ from a biomass-fueled combustion power plant range from \$150 to \$400 per metric ton of $CO_2$.[11] Furthermore, purification expenses for this procedure are projected to be between \$70 and \$275 per metric ton of $CO_2$.[11] Despite the implementation of costly purification procedures, trace amounts of contaminants persist in the gas feed.[12,13] Contaminants can pose a significant challenge to the long-term operation of Ag catalysts in industrial applications. Hence, it is crucial to study the $CO_2$ reduction reaction ($CO_2$RR) on Ag catalysts in the presence of varying concentrations of impurities. Furthermore, it is also important to develop strategies for protecting the catalysts from exposure to impurities and alleviating the poisoning issue.

Unprocessed flue gas emissions contain various gaseous impurities, the concentration of each impurity significantly depends on the emission source and, hence, the type of industry. Typically, flue gas emitted from power plants contains impurities such as sulfur oxides ($SO_x$), nitrogen oxides ($NO_x$), oxygen, and volatile organic compounds (VOC).[14,15] Hee Ko *et al.* have studied the impact of nitrogen oxides on electrochemical $CO_2$RR.[16] They used various $NO_x$ (including NO, $NO_2$, and $N_2O$) on Cu, Ag, and Sn catalysts in a flow cell and found that the presence of $NO_x$ (up to

[a] *Department of Chemical Engineering, Faculty of Applied Sciences, Delft University of Technology, Van der Maasweg 9, 2629 HZDelft, The Netherlands. E-mail: M.Li-5@tudelft.nl, J.R.vanOmmen@tudelft.nl*
[b] *Process & Energy Department, Faculty of Mechanical Engineering, Delft University of Technology, Leeghwaterstraat 39, 2628 CB Delft, The Netherlands*

† Electronic supplementary information (ESI) available. See DOI: https://doi.org/10.1039/d4cy01196a

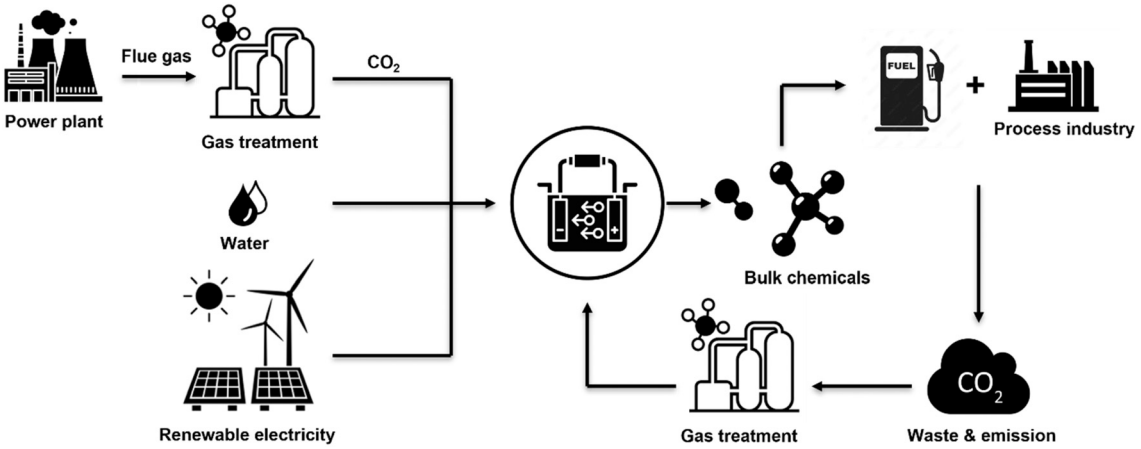


Fig. 1 Schematic illustration of the concept for $CO_2$ electroreduction in industry.

0.83 vol%) in the $CO_2$ feed results in a notable reduction in Faradaic efficiency (FE) during $CO_2$ electroreduction. This reduction is attributed to the preferential electroreduction of $NO_x$ over $CO_2$. However, despite the decrease in FE, when the pure $CO_2$ feed is restored, the electrocatalyst maintains similar $CO_2$ reduction capabilities. This indicates that the enduring impact of $NO_x$ on the catalytic performance of the modeled catalysts is negligible over the long term. Xu *et al.* found that when $O_2$ impurities are present at typical concentrations (4 vol% of $O_2$), most of the current was redirected from $CO_2$RR towards the oxygen reduction reaction (ORR).[17] This poses more serious issues when operating at elevated pressures. For example, 99% of the current was redirected to ORR at 15 bar. Van Daele *et al.* studied the stability of Ag and $Bi_2O_3$ catalysts with 198 ppm $SO_2$ in $CO_2$ and 213 ppm NO in $CO_2$ over the course of 20 h.[18] They found that the studied catalysts have a stable performance and high Faradaic efficiencies towards the target products over 20 h. Therefore, it seems that operating with 200 ppm of NO and $SO_2$ in the gas feed will not have much effect on the catalyst during $CO_2$RR. However, the presence of oxygen will significantly suppress the FE towards target products during $CO_2$RR; with 1 vol% of $O_2$ added to the stream, 23% of the FE towards $CO_2$RR was lost. This likely is due to the fact that the oxygen impurity has a higher concentration than NO and $SO_2$, and the preferential reduction of $O_2$ compared to $CO_2$ during the reaction. Albertini *et al.* found that using a passivation layer such as metallic oxides coatings can preserve catalyst's activity and improve its stability for $CO_2$ reduction.[19] Based on the aforementioned reports, we may infer that the impurities primarily affect the $CO_2$RR through competing reactions, rather than the poisoning effects that will lead to a long-term influence on the catalysts. Moreover, these studies are all carried out in flow cell reactors, while an H-cell system may give additional insights, as it can provide additional perspectives into the intrinsic properties of the catalyst by decoupling some of the complexities introduced in flow cells.

The objective of this paper is to determine the effect of $SO_2$ impurities on the Ag catalyst for the electrochemical reduction of $CO_2$ in two different cell geometries: an H-cell and a membrane electrode assembly (MEA) cell. We select $SO_2$ as the impurity for this study since it is found in most flue gases and sulfur has a pronounced poisoning effect on Ag catalysts.[7–9] We find that $SO_2$ has a more pronounced impact on Ag on carbon black (Ag/CB) catalysts in the H-cell compared to in the MEA reactor. This is attributed to the higher solubility of $SO_2$ in the electrolyte compared to $CO_2$, leading to an accumulation effect in the H-cell. This causes a higher $SO_2$ concentration near the electrode surface in the H-cell system than in the MEA reactor system. We use thermal atomic layer deposition (ALD) to deposit $SiO_2$ on Ag/CB catalyst to protect it from $SO_2$ impurities. ALD is a gas phase coating technique based on the alternating use of two reactants, depositing a thin film on a substrate. It provides sub-nanometer precision in coating thickness, controlled by the number of deposition cycles.[20] After applying 2 to 8 cycles of $SiO_2$ ALD providing a nanocoating on the outer surface of the Ag/CB catalyst, the effect of $SO_2$ on the selectivity of the catalyst is diminished at less negative potentials. This is attributed to the permeability difference between $CO_2$ and $SO_2$ through $SiO_2$ coatings.

## Experimental

### Materials

Silicon tetrachloride ($SiCl_4$, 99%) and iridium oxide ($IrO_2$) were purchased from Alfa Aesar, isopropanol (≥98%) was purchased from Honeywell, Nafion™ perfluorinated resin solution (5 wt% in lower aliphatic alcohols and 15–20% water) was purchased from Sigma-Aldrich. Deionized water with a resistivity of 18 MΩ cm was used as the co-reactant for ALD. 20 wt% of Ag on Carbon black-Vulcan XC 72R catalyst, Carbon Black Vulcan XC 72R, and Sigracet 39BB carbon paper gas diffusion layers (GDL) pretreated with PTFE in microporous layer were purchased from FuelCell store. Glassy carbon plates were ordered from HTW Hochtemperatur-

Werkstoffe GmbH (Germany). The electrolyte solution was prepared from ultrapure water (Milli-Q IQ 7000, 18.2 MΩ cm). PiperION® anion exchange membrane, 20 microns, was purchased from FuelCell store and submerged in the electrolyte overnight prior to MEA experiments. Potassium bicarbonate ($KHCO_3$, 99.95%) was purchased from Sigma-Aldrich. Anion exchange membrane (Selemion AMV) was purchased from AGC Engineering and kept in deionized water after receiving, and used for H-cell experiments. Ag nanopowder with a particle size from 20–40 nm and without oxide layer was purchased from Thermo Fisher Scientific. All chemicals were received and used without further purification.

## Electrode preparation

**Electrodes used in H-cell experiments.** The Ag/CB catalyst was first drop casted on the glassy carbon electrode before the ALD coating. The catalyst ink was prepared by combining 4 mg of catalyst with 800 μL of deionized water, 180 μL of isopropanol, and 20 μL of Nafion perfluorinated resin solution in a vial. The mixture was then sonicated in an ice bath for 1 hour. Following this, 25 μL of the catalyst ink was drop-cast onto the surface of the glassy carbon electrode each time and this process was repeated four times to achieve a homogeneous deposition on the electrode. The $SiO_2$ coatings on the catalyst were then deposited in a custom-built flat substrate ALD reactor[20–22] operating at atmospheric pressure. The reactor chamber comprises a metal cylinder with an inner diameter of 40 mm and a length of 190 mm, accompanied by a substrate holder with dimensions of 30 mm by 125 mm. To ensure a uniform temperature profile, the deposition temperature was monitored and regulated using two thermocouples positioned inside and outside the ALD reactor. We opted for atmospheric pressure ALD over vacuum ALD as it reduces investment costs and enhances throughput at a larger scale.[21,22] Our $SiO_2$ deposition process was adapted from literature,[23] but the reaction time and precursor gas flow rate were adjusted based on our own requirements and still under the saturation conditions.[24] In summary, the $SiCl_4$ and $H_2O$, the ALD reactants, were filled in stainless steel bubblers and kept at room temperature. Nitrogen gas, with a purity of 99.999%, served as both carrier and purging gas, flowing at a rate of 0.5 L $min^{-1}$ throughout the process, parallel to the substrate surface in the reactor. Before each experiment, samples underwent air plasma pre-treatment at room temperature and 4 mbar pressure for 60 seconds using a Harrick plasma machine. The ALD reactor was heated to and maintained at 100 °C throughout the process. $SiCl_4$ was introduced into the reactor for 15 second pulses, followed by 60 second purging with $N_2$ and 30 second dosing of $H_2O$ vapor. A final 60 second purging with $N_2$ completed one ALD cycle. Detailed $SiO_2$ ALD operation conditions are available in Table S1.† Samples with varying numbers of ALD cycles were obtained by repeating the ALD cycles as needed. Upon completion of the synthesis process, the reactor was purged with $N_2$ flow for 15 minutes and cooled to room temperature.

**Electrodes used in MEA experiments.** The catalyst used during the MEA experiments was synthesized using a vibrated fluidized bed reactor[25–27] operating at atmospheric pressure. A vibrating table was used at a frequency of 60 Hz to fluidize the powders and create uniform fluidization inside the reactor during the reaction. A glass column with an inner diameter of 2.5 cm was used as the reactor. 0.5 g of Ag/CB catalyst (pre-dried at 80 °C for 3 hours before the experiment, to remove the moisture) was used for each synthesis batch in the reactor. The $SiCl_4$ and $H_2O$, the ALD reactants, were filled in stainless steel bubblers and kept at room temperature. Nitrogen gas, with a purity of 99.999%, served as both carrier and purging gas throughout the reaction. A compensation $N_2$ stream with a flow rate of 1.5 L $min^{-1}$ was employed during the $SiCl_4$ dosing period to maintain an equal gas flow of 2 L $min^{-1}$ throughout the whole ALD process and keep the fluidization of the powders inside the reactor. The ALD reactor was heated to and maintained at 100 °C throughout the process. $SiCl_4$ was introduced into the reactor for 60 second pulses, followed by 150 second purging with $N_2$ and 60 second dosing of $H_2O$ vapor. A final 150 second purging with $N_2$ completed one ALD cycle. By repeating the same ALD cycles for 4 times, 4 cycles coated sample was achieved. After the synthesis procedure, the fluidized bed reactor was purged for 15 minutes with $N_2$ flow to remove the residual reactants. Detailed $SiO_2$ ALD operation conditions were shown in Table S1.† The 4 cycles $SiO_2$ coated Ag/CB powders synthesized using the aforementioned method was utilized to prepare the ink that can be airbrushed on the GDL for the MEA experiments. The ink formula is very similar to the previously mentioned ink formula used for the H-cell experiments. In general, 4 mg of catalyst with 800 μL of isopropanol, 180 μL of deionized water, and 20 μL of Nafion perfluorinated resin solution were mixed in a vial. The mixture was then sonicated in an ice bath for 1 hour. After that, the ink solution was airbrushed onto the GDL using an airbrush gun and $N_2$ flow to reach a catalyst loading of 0.2 mg $cm^{-1}$.

**Gas mixing steps for $SO_2$ impurities experiments.** A gas mixing apparatus (Environics® Series 4000) was employed to mix the feed gas and ensure precise control over gas proportions for the electrochemical tests. To protect against the potential corrosion induced by $SO_2$, a precautionary measure was taken by coating the mass flow controllers and gas tubing within the testing system with SilcoNert® and sealing them with Kalrez®. The generation of varied concentrations of $SO_2$ gas was achieved by using two standard gas cylinders containing $SO_2$ with concentrations of 100 ppm and 10 000 ppm, balanced with $CO_2$ from Linde Gas. The pure $CO_2$ gas used in the experiments was also from Linde Gas with a purity of 99.999%. Detailed information regarding the gas recipes used for the electrochemical tests can be found in Table S2.†

**Material characterization.** X-ray photoelectron spectroscopy (XPS) analyses were conducted utilizing the Thermo Scientific™

 

K-alpha™ instrument from ThermoFisher™ Scientific. The instrument employed monochromatic X-ray beams of aluminum Kα radiation (1486.7 eV) with a spot size of 400 μm. For the survey scans, a pass energy of 200 eV and a step size of 1 eV were employed, while higher-resolution spectra were obtained using a pass energy of 50 eV and a step size of 0.1 eV. All peak positions were analyzed and calibrated with reference to the aliphatic C 1s peak at 284.8 eV, utilizing CasaXPS software.

XPS area scan was performed with a Thermo Scientific™ K-alpha™ (ThermoFisher™ Scientific) utilizing a monochromatic X-ray of aluminum Kα radiation (1486.7 eV) and a circular area was chosen with a diameter of 12 mm. 121 points were selected and evenly distributed within the circular area. A pass energy of 153 eV and a dwell time of 0.5 s were used. The data was analyzed and plotted using the Avantage software.

### Electrochemical measurements

**Electrochemical measurements in H-cell.** The electrochemical measurements were conducted using a H-cell setup.[28] A leak-free Ag/AgCl reference electrode (sat. KCl) was employed, alongside a counter electrode consisting of $IrO_2$-coated glassy carbon electrode. All potentials employed in this study were adjusted to the RHE scale using the following equation:[29]

$$E_{RHE} = E_{Ag/AgCl} + 0.197 + 0.059 \times pH$$

A 0.1 M solution of $KHCO_3$ served as the electrolyte in both chambers, and each chamber contains 1.8 mL of electrolyte. An anion-exchange membrane, Selemion AMV, was utilized to separate the anode and cathode chambers of the H-cell. Electrochemical measurements were conducted using a Biologic SP-200 potentiostat. Potentiostatic electrochemical impedance spectroscopy was utilized to evaluate the ohmic loss of the cell and was compensated for each experiment. Chronoamperometric measurements were carried out at different applied potentials from −0.8 to −1.2 V *vs.* RHE and were used to determine the FE of the catalysts. Before each experiment, the cathode electrolyte was purged with feeding gas for 15 minutes. The gas products were analyzed by an in-line gas chromatography (GC) (Compact GC4.0, Global Analyzer Solutions). Every 2 minutes the products were analyzed by the GC for quantification. The gas flow rate used during the experiments was kept at 8 sccm for every tests.

**Electrochemical measurements in MEA.** The electrochemical measurements were conducted using a MEA reactor purchased from Dioxide Materials. It is a 5 $cm^2$ $CO_2$ MEA electrolyzer cell coupled with a stainless steel flowfield plate with a serpentine channel in contact with the cathode GDE and a titanium flowfield plate with a serpentine channel in contact with the anode GDE. The reactor was assembled with 2 N*m Torque to ensure a leak-free assembly. The working electrode was prepared using the aforementioned method. The counter electrode was an $IrO_2$ airbrushed GDE. The anion-exchange membrane used in the MEA was a PiperION® anion exchange membrane. 40 ml of 1 M $KHCO_3$ solution was used and circulated with a flow rate of 5 ml $min^{-1}$ in the anode serpentine channel. Use of 0.1 M $KHCO_3$ electrolyte in H-cell configurations and 1 M $KHCO_3$ electrolyte in MEA configurations are widely reported in the literature and facilitates comparisons across different studies. Employing 0.1 M $KHCO_3$ electrolyte in the MEA configuration can result in a very high Faradaic efficiency toward $H_2$ and a significantly low FE toward CO, thereby diminishing its relevance for $CO_2$ reduction studies. Chronopotentiometry measurements were carried out at different current densities and were used to determine the FE of the catalysts. The current density was calculated by dividing the applied current by the geometric area of the working electrode. CV measurements were carried out from 0.2 V to −1.0 V at a scan rate of 10 mV $s^{-1}$. The gas products were analyzed using the same in-line GC as described in the H-cell experiments; the gas flow rate used during the experiments was 20 sccm for every test.

## Results and discussion

### $SO_2$ impurities effects on $CO_2$ electroreduction in H-cell reactor

We first examined the effect of $SO_2$ impurities on the Ag/CB catalyst for $CO_2$ electroreduction in the H-cell system. A series of Ag/CB samples coated with $SiO_2$ were synthesized using ALD with a flat substrate reactor and compared with an uncoated Ag/CB sample. As demonstrated in our previous study,[30] thick $SiO_2$ coatings can reduce the catalyst activity. Therefore, in this study, we limited the deposition to a maximum of 8 cycles to avoid compromising catalyst performance. Based on the reported growth per cycle of $SiO_2$ using $SiCl_4$ under the experimental conditions, which is approximately 2 Å per cycle,[31,32] a very thin $SiO_2$ layer ranging from 0.4 nm to 1.6 nm is anticipated after 2 to 8 cycles of ALD coating. To determine the actual Ag weight percentage in the original Ag/CB nanoparticles, the sample underwent characterization through thermogravimetry differential thermal analysis (TG/DTA). The TG/DTA analysis (Fig. S1†) showed that roughly 22 wt% of $Ag_2O$ residues were present after the analysis and revealed approximately 20 wt% of Ag in the original Ag/CB samples, and this number matches the metal loading specified in the documentation from the supplier. The rate of $SiO_2$ deposition was characterized *via* X-ray photoelectron spectroscopy (XPS), with Fig. S2† illustrating a monotonic increase in Si atomic percentage with the number of ALD cycles. High-resolution Si 2p spectra indicated that the Si in the coated samples predominantly exists in the $SiO_2$ state, which can be deconvoluted into Si 2p3/2 and Si 2p1/2 peaks. This demonstrated successful $SiO_2$ deposition on the surface of Ag/CB samples, with the Si content increasing proportionally with the number of coating cycles.

The stability of the original Ag/CB catalyst was assessed in an H-cell at −1.0 V *vs.* RHE over a 20 hour period. Fig. 2 shows that the Faradaic efficiency (FE) of the original Ag/CB catalyst towards CO remained relatively constant at around 70% throughout the 20 hour test, with minor fluctuations. The total Faradaic efficiency falling below 100% can be attributed to incomplete product detection and electron losses resulting from parasitic processes, such as electrode corrosion and catalyst degradation. This underscores the stability of the original Ag/CB catalyst in H-cell environments, consistent with previous research, indicating the robustness of Ag catalysts under similar testing conditions.[2–5] Notably, the Ag catalyst exhibited no significant deterioration in performance under neutral pH conditions. However, the selectivity of the original Ag catalyst was found to be lower than that reported in some papers.[2,33,34] To further investigate the selectivity of the Ag catalyst, we also evaluated pure Ag nanoparticles drop-casted onto a glassy carbon electrode while maintaining consistent metal loading (80 μg $cm^{-2}$) with our Ag/CB catalyst. As depicted in Fig. S3,† an optimal $FE_{CO}$ of the pure Ag nanoparticles was achieved at −0.8 V *vs.* RHE, with a similar selectivity towards CO of around 70%. Upon mixing the Ag nanoparticles with carbon black to mimic our Ag/CB catalyst while keep the same Ag loading on the electrode, we observed that the optimal FE was achieved at −1.0 V *vs.* RHE, demonstrating a $FE_{CO}$ of approximately 72%. This indicated that the low FE of the Ag catalyst was not inherent to the catalyst itself but was more associated with the used H-cell configuration. In the H-cell configuration, the availability of $CO_2$ in the cathode compartment was restricted due to the low solubility of $CO_2$ in the electrolyte. The low solubility of $CO_2$ resulted in a low concentration of $CO_2$ in the vicinity of the electrode. When the $CO_2$ concentration near the cathode is insufficient, the $FE_{CO}$ decreases. $CO_2$ must then diffuse through the electrolyte to reach the cathode, and in the H-cell configuration, this diffusion is hindered by the distance between the $CO_2$ source (*e.g.*, the gas phase or $CO_2$ inlet) and the cathode. The slower diffusion rate can lead to localized $CO_2$ depletion at the electrode, further restricting $CO_2$ reduction efficiency. Mass transfer, including the movement of $CO_2$ to the electrode, is also limited in the H-cell configuration due to the static nature of the electrolyte and the lack of continuous flow. These limitations were more serious under high current densities, as these conditions require a higher amount of $CO_2$ supply. Consequently, $CO_2$ reduction in the H-cell was less efficient, resulting in lower FE towards CO. While the partial current density of the Ag nanoparticles with or without mixing with carbon black towards CO appeared comparable at all three potentials, there was a notable disparity in the $H_2$ partial current density between the Ag nanoparticles drop casted directly on the glassy carbon electrode and those mixed with carbon black. The Ag nanoparticles mixed with carbon black consistently exhibited a lower $H_2$ partial current density at all three potentials. We hypothesize that part of the Ag is buried beneath the carbon particles. This means that the $CO_2$ consumption during $CO_2$ reduction will be lower with these samples. Therefore, the samples with carbon black will have a relatively higher $CO_2$ concentration near the electrode, which suppresses the hydrogen evolution activity.

$SO_2$ concentrations of 10 ppm, 100 ppm, and 1000 ppm were tested in this study, considering that the majority of flue gas

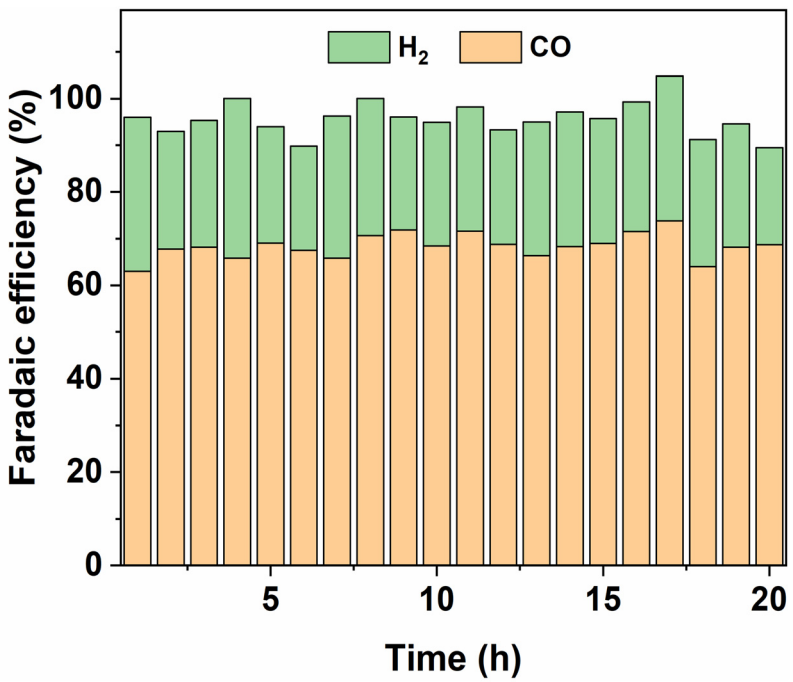


Fig. 2 Faradaic efficiency toward $H_2$ and CO of the uncoated Ag/CB catalyst during 20 h H-cell testing at −1.0 V *vs.* RHE using a pure $CO_2$ gas feed and a 0.1 M $KHCO_3$ electrolyte.

 

emissions from power plants typically fall within an $SO_2$ concentration range from 100 to 400 ppm.[18] The gas compositions employed for the $SO_2$ impurity experiments are listed in Table S2.† Three different $CO_2$ gas cylinders containing 0, 100, and 10 000 ppm $SO_2$ were utilized, and a gas mixer was employed to ensure thorough mixing of various gas streams to achieve a homogeneous gas stream flowing into the H-cell cathode chamber. The original Ag/CB catalyst (*i.e.*, 0 cycles) and catalysts with 2, 4 and 8 cycles of $SiO_2$ ALD coating were tested at three potentials using chronoamperometry (CA) under different gas feed compositions. As is seen from Fig. 3, the catalyst performance was first benchmarked with a pure $CO_2$ feed and a similar selectivity toward CO was observed with and without $SiO_2$ coating, reaching the highest $FE_{CO}$ of 70% at −1.0 V *vs.* RHE. Nevertheless, when $SO_2$ impurities were introduced into the gas stream, the $FE_{CO}$ of the uncoated Ag/CB catalyst showed a significant decrease. A decrease in $FE_{CO}$ to 57% with 10 ppm $SO_2$ and 56% with 100 ppm $SO_2$, at −1.0 V *vs.* RHE was observed. At the highest $SO_2$ concentration (1000 ppm), the $FE_{CO}$ decreased by 23%, 24%, and 14% at −0.8 V *vs.* RHE, −1.0 V *vs.* RHE, and −1.2 V *vs.* RHE, respectively. The $SO_2$ poisoning effect on the Ag catalyst appears to be potential dependent, with a greater impact observed at lower potentials. This is expected due to the more favorable reduction of $SO_2$ over $CO_2$, since $SO_2$ reduction has a significantly less negative reduction potential compared to $CO_2$ reduction.[35] We have conducted cyclic voltammetry tests under various gas supplies, including pure Ar, $CO_2$ with 1000 ppm $SO_2$ and pure $CO_2$ to verify the $CO_2$ reduction potential and the $SO_2$ reduction potential. However, as shown in Fig. S4,† no distinct $SO_2$ reduction peak was observed. This indicates that $SO_2$ reduction occurs within a potential window similar to that of $CO_2$ reduction and hydrogen evolution. When we calculate the loss in $FE_{CO}$ and attribute it to $SO_2$ reduction, we find that approximately 50 ppm $SO_2$ is required to account for the missing FE when 1000 ppm $SO_2$ is introduced at −0.8 V *vs.* RHE. This suggests that there is sufficient $SO_2$ in the gas stream during the reaction for the indicated $SO_2$ reduction (detailed calculation method can be found in ESI,† method to calculate the $SO_2$ concentration required to get $SO_2$ reduction section). Additionally, the potential poisoning of the Ag/CB catalyst during the reaction can also contribute to the performance degradation when $SO_2$ is introduced to the gas stream, as we detected the formation of $Ag_2S$ species on the surface of the catalyst after the reaction, as shown in Fig. 4. Although the exact mechanism of the $Ag_2S$ formation process is unclear and remains an objective for future study. All of these factors combined together contribute to the decrease in $FE_{CO}$ for the $CO_2$ electrolysis. The decrease in CO selectivity of the Ag/CB catalyst at a high concentration of $SO_2$ impurities was more pronounced at less negative potential (−0.8 V *vs.* RHE) compared to more negative potential (−1.2 V *vs.* RHE) indicating that the competition between $SO_2$ reduction and $CO_2$ reduction is potential dependent. $SO_2$ reduction is more favored compared to $CO_2$ reduction at less negative potentials. As the potential becomes more negative, the effectiveness of $CO_2$ reduction increases, with the loss in $FE_{CO}$ decreasing. The Ag/CB catalysts protected with 2–8 ALD cycles of $SiO_2$ coating were much less affected by the $SO_2$

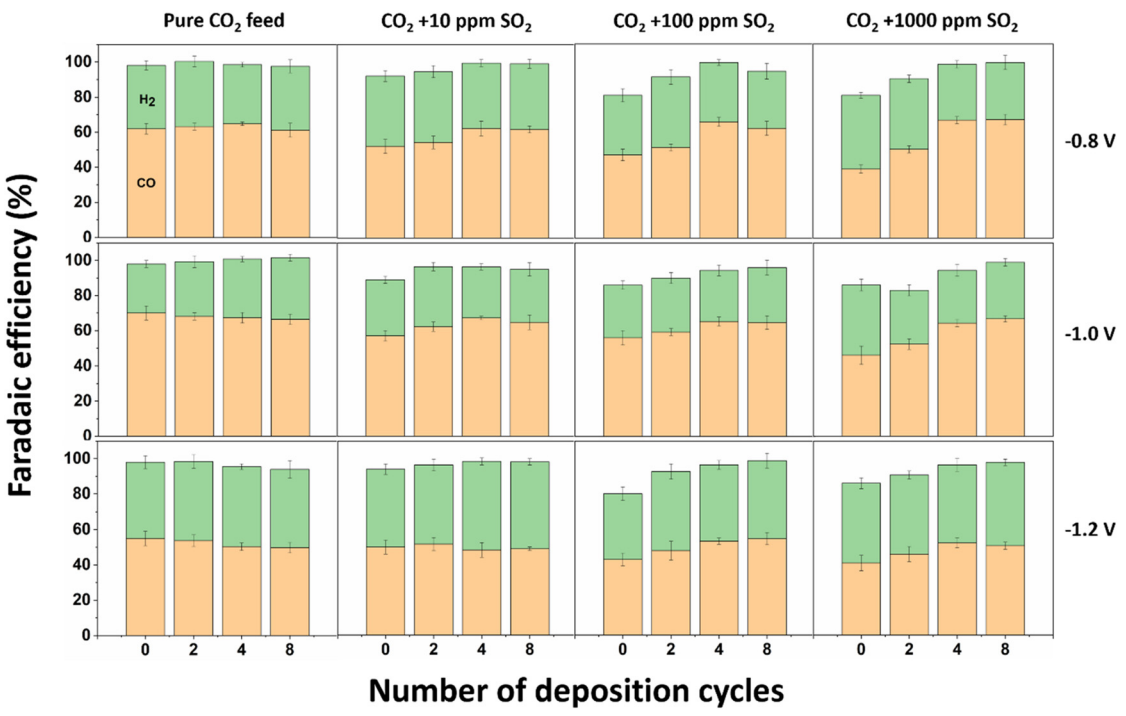


**Fig. 3** Faradaic efficiency of the Ag/CB catalyst with or without $SiO_2$ coating during 1 h H-cell CA testing in a 0.1 M $KHCO_3$ electrolyte at 3 potentials using $CO_2$ gas feed with different concentrations of $SO_2$ impurities. The data was collected from two independent measurements and the error bars represent the arithmetic mean.

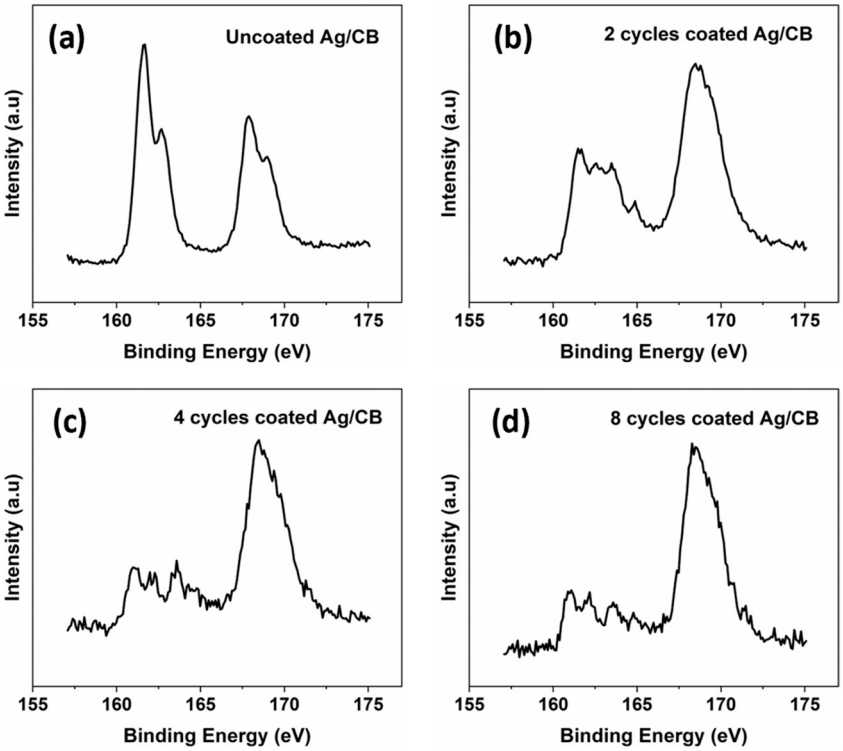


Fig. 4 S 2p XPS spectrum of the Ag/CB catalyst after $CO_2$ electrolysis with 1000 ppm $SO_2$. (a) Ag/CB catalyst without $SiO_2$ coating. (b) Ag/CB catalyst with 2 cycles $SiO_2$ coating. (c) Ag/CB catalyst with 4 cycles $SiO_2$ coating. (d) Ag/CB catalyst with 8 cycles $SiO_2$ coating, tested at H-cell at −1.0 V *vs.* RHE.

contaminant. At −0.8 V *vs.* RHE, the $FE_{CO}$ of the uncoated Ag/CB catalyst was 52%, 47%, and 39% with 10 ppm $SO_2$, 100 ppm $SO_2$, and 1000 ppm $SO_2$, respectively. After applying 2 cycles of $SiO_2$ coating on the surface of the catalyst, the $FE_{CO}$ improved to 54%, 51%, and 50%, respectively. When we further increased the coating cycles to 4 cycles, the $FE_{CO}$ of the ALD coated catalyst increased to 62%, 65%, and 66%. After 8 cycles of $SiO_2$ coating, the $FE_{CO}$ reached 62%, 62%, and 67%. The $SiO_2$ coating thereby effectively reduced the $SO_2$ poisoning effect on the Ag catalyst. When the applied potential became more negative, the $SO_2$ effects on Ag catalyst decreased, and the coating effectiveness decreased as well. The $FE_{CO}$ of the uncoated Ag/CB catalyst at −1.2 V *vs.* RHE was 50%, 43%, and 41% under 10 ppm $SO_2$, 100 ppm $SO_2$, and 1000 ppm $SO_2$, respectively. After 2 cycles of coating, the $FE_{CO}$ improved to 51%, 48%, and 46%. And after 4 cycles coating, it increased to 48%, 53%, and 52%. With 8 cycles coating, the $FE_{CO}$ improved to 49%, 54%, and 50%. The decreased $FE_{CO}$, especially for the uncoated and 2 cycles coated samples under $SO_2$ impurity, can likely be attributed to the $SO_2$ reduction and the poisoning of the catalysts. However, due to the high solubility of the sulfur-containing anions in the electrolyte and its cross-over through the anion-exchange membrane to the anolyte, we cannot accurately detect the $SO_2$ reduction products and quantify their Faradaic efficiency.

Fig. 4 presents the XPS characterization of the Ag/CB catalyst without and with $SiO_2$ coating following a 1 hour CA test at −1.0 V *vs.* RHE with 1000 ppm $SO_2$. In all samples, an intense peak at 168.7 eV was observed in the S 2p spectrum, attributed to the sulfur-containing functional groups within the Nafion binder utilized for drop-casting the catalyst on the surface of the glassy carbon electrode, and serving as the ionomer in the catalyst. Peaks at 161.1 eV and 162.2 eV are attributed to silver sulfide ($Ag_2S$) formation during the reaction.[36] Notably, the intensity of the $Ag_2S$ peaks was notably higher in the uncoated catalyst. Upon applying 2–8 cycles of $SiO_2$ coating, a decrease in the intensity of the $Ag_2S$ peak was observed, suggesting that $SiO_2$ coating mitigated $Ag_2S$ formation during the reaction under high concentrations of $SO_2$ (1000 ppm $SO_2$) gas feed. An XPS area scan was conducted after 1 h $CO_2$ electrolysis at −1.0 V *vs.* RHE with 2 kinds of gas feed. Fig. S5† shows that the uncoated Ag/CB catalyst after 1 h $CO_2$ electrolysis with pure $CO_2$ gas feed only has a low intensity of S peak on the electrode. For a gas feed of $CO_2$ with 1000 ppm $SO_2$, the uncoated Ag/CB catalyst shows a much stronger S peak on the electrode. Nevertheless, for the catalyst treated with 8 cycles of $SiO_2$ coating, the S peak is significantly decreased on the electrode after $CO_2$ electrolysis with 1000 ppm $SO_2$.

In summary, we found that the Ag/CB catalyst was significantly affected by $SO_2$ impurities in the H-cell geometry, especially for a high $SO_2$ concentration and at a less negative potential. The $SiO_2$ coating can be used to protect the Ag/CB catalyst from $SO_2$ impurities and maintain the catalyst selectivity for all investigated potentials.

### $SO_2$ and $CO_2$ permeability differences through $SiO_2$ coating

To further illustrate the protection mechanism of $SiO_2$ on Ag/CB catalysts against $SO_2$ impurities, we investigated the

 

permeability differences of $SO_2$ and $CO_2$ through $SiO_2$ coatings based on existing papers. Mohd Nor *et al.* found that $CO_2$ has high permeability through $SiO_2$ modified polymer matrix membranes.[37] After adding 5 wt% of $SiO_2$ nanoparticles to the polymer matrix membranes (ENR/PVC), the $CO_2$ gas permeability increased to approximately 6 times higher than the original membranes without $SiO_2$ modification. Wahab *et al.* also found a similar phenomenon.[38] They reported that $CO_2$ gas exhibits strong interaction with $SiO_2$ due to the presence of hydroxyl functional groups (–OH) on the $SiO_2$ particles. This interaction enhances the solubility of $CO_2$ within the membrane, thereby improving $CO_2$ diffusivity and resulting in high permeability of $CO_2$ through $SiO_2$ filled fiber mixed matrix membrane. Meng *et al.* tested that the organic–inorganic hybrid $SiO_2$ membranes exhibited a high $O_2$ permeance that was $2.87 \times 10^{-8}$ mol $m^{-2}$ $s^{-1}$ $Pa^{-1}$ and a poor $SO_2$ permeance of $3.9 \times 10^{-9}$ mol $m^{-2}$ $s^{-1}$ $Pa^{-1}$.[39] The $O_2$ permeance was 7.4 times higher than the $SO_2$ permeance through the membranes. This indicates that the $SO_2$ permeability through this organic–inorganic hybrid $SiO_2$ membranes is very low. Yoshiura *et al.* also found that the 3,3,3-trifluoropropyltrimethoxysilane derived $SiO_2$ membranes have very high $SO_4^{2-}$ ions rejection rates.[40] The $NaSO_4$ and $MgSO_4$ rejection percentage after the liquid permeation tests was 91.0% and 98.2%, respectively. This is attributed to the dissociation of the –OH groups on the silica surface during testing and produce a negatively charged surface. The $SiO_2$ coating on the Ag/CB catalyst was negatively charged during $CO_2$RR as well. Hence, it can also have a repulsive effect on $SO_2$ derived ions. Yu *et al.* discovered that silica–zirconia membranes with a high Si/Zr molar ratio (Si/Zr = 7/3) exhibit excellent resistance to $SO_3$ and demonstrate gas separation of $O_2/SO_3$ selectivity ranging from 13 to 10, surpassing the Knudsen selectivity of 1.58.[41] This suggests promising potential for their application in $O_2/SO_3$ separation processes and indicates that $O_2$ has more than 10 times higher permeability through silica–zirconia membranes with a high Si/Zr molar ratio compared to $SO_3$. Based on the preceding discussion, it can be inferred that there is a notable difference in the permeability of $CO_2$ and $SO_2$ through $SiO_2$, with $CO_2$ showing significantly higher permeability compared to $SO_2$ or $SO_2$ derived ions present in the electrolyte. The variation in permeability between $CO_2$ and $SO_2$ indicates that the concentrations of these gases outside and inside the $SiO_2$ coating, which directly interact with the Ag/CB catalyst, are also likely to differ. The lower $SO_2$ concentration on the inside of the coating may account for the observation that after applying 2–8 cycles of $SiO_2$ coating, the formation of $Ag_2S$ on the electrode surface is considerably less than without $SiO_2$ coating after $CO_2$ electrolysis with 1000 ppm $SO_2$ feed at −1.0 V *vs.* RHE. It also explains why $SO_2$ has much less effect on the catalyst's selectivity after it has been coated with $SiO_2$ films. The $SO_2$ concentration near the electrode surface decreases, so the competition between the $SO_2$ reduction and $CO_2$ reduction is reduced, and the potential poisoning of the Ag/CB catalyst is minimized.

### $SO_2$ impurities effects on $CO_2$ electroreduction in MEA reactor

Based on the findings from our investigation using the H-cell, we proceeded to evaluate the performance of $SiO_2$ coated Ag/CB samples in a MEA reactor, a widely utilized flow cell structure in the field of $CO_2$ reduction, to understand their behavior in the flow cell system. Given that the current density in the H-cell is relatively low and cannot meet industrially relevant requirements, assessing the $SiO_2$ coated Ag/CB catalyst in a flow cell geometry such as a MEA is needed.

We applied 4 cycles of $SiO_2$ coating on Ag/CB powders using a fluidized bed ALD reactor. This is different from the samples used in H-cell tests, in which we used a flat substrate ALD reactor and only coated the very outermost surface of the Ag/CB catalyst on the glassy carbon electrode. For these experiments, we fluidized the Ag/CB powder in a dedicated ALD reactor and coated the entire surface of the Ag/CB particles. The coated Ag/CB catalyst was airbrushed on the gas diffusion electrode and assembled in the MEA electrolyzer for the electrochemistry tests. The uncoated Ag/CB catalyst tested in MEA showed a $FE_{CO}$ of 79% at 100 mA $cm^{-2}$ with a pure $CO_2$ gas feed (as shown in Fig. 5a). When the gas feed shifted to $CO_2$ with 1000 ppm $SO_2$, the $FE_{CO}$ did not decrease significantly as in the experiments in the H-cell, but remained at a $FE_{CO}$ of 75%. When the Ag/CB catalyst was coated with 4 cycles of $SiO_2$, we observed that the catalyst's selectivity was inhibited to some extent. The 4 cycles $SiO_2$ coated sample showed a $FE_{CO}$ of 70% with pure $CO_2$ feed, and a $FE_{CO}$ of 71% when the gas feed was changed to $CO_2$ combined with 1000 ppm $SO_2$. The slight inhibition effect of the coating may stem from the $SiO_2$ coating forming connections between catalyst particles, which could hinder electrical conductivity and ionic charge transfer between the membrane and the bulk catalyst. The water transport within the bulk catalyst might also be influenced by the $SiO_2$ coating. All of these factors can collectively affect the catalyst's selectivity in the MEA configuration. Fig. S6† shows that the CV scan of the uncoated Ag/CB catalyst and the catalyst with 4 cycles of $SiO_2$ coating do not have notable differences. The oxidation and reduction peaks of Ag are well defined with 4 cycles of $SiO_2$ coating and nearly coincide with the catalyst without coating. This indicates that the obstruction caused by the $SiO_2$ coating on the catalyst's outmost surface active sites is minimal. Fig. 5b and c shows the chronopotentiometry (CP) results of the Ag/CB catalyst tested at 100 mA $cm^{-2}$. It indicates that adding 1000 ppm $SO_2$ to the feeding gas does not change the cell potential under the same current density. Applying an $SiO_2$ coating also did not alter the cell potential for the same current density. The XPS characterization of the catalyst before and after $CO_2$ electrolysis with or without $SO_2$ impurities are

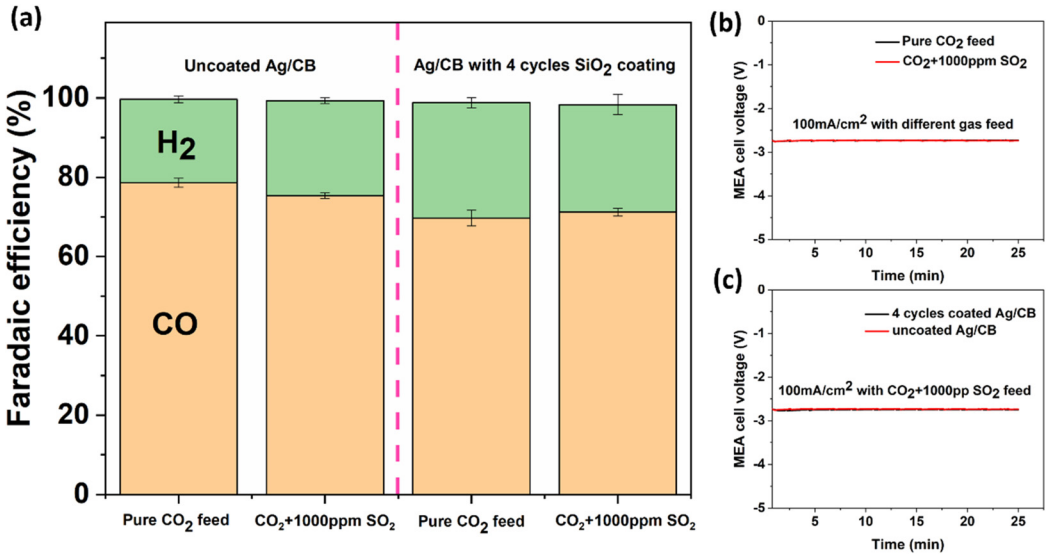


**Fig. 5** (a) Faradaic efficiency of the Ag/CB catalyst with or without $SiO_2$ coating tested at MEA reactor at 100 mA $cm^{-2}$ current density in a 1 M $KHCO_3$ electrolyte with pure $CO_2$ feed or $CO_2$ mixed with 1000 ppm $SO_2$. The data was collected from two independent measurements and the error bars represent the arithmetic mean. (b) CP testing of the Ag/CB catalyst at MEA reactor. Original Ag/CB catalyst tested with pure $CO_2$ or $CO_2$ with 1000 ppm $SO_2$ impurities at 100 mA $cm^{-2}$ current density. (c) CP testing of the Ag/CB catalyst at MEA reactor. Ag/CB catalyst with or without 4 cycles of $SiO_2$ coating tested using $CO_2$ with 1000 ppm $SO_2$ impurities as gas feed at 100 mA $cm^{-2}$ current density.

shown in Fig. 6. From the figure we observe that peaks at 161.1 eV and 162.2 eV, which are attributed to $Ag_2S$, are present in all samples, even with pure $CO_2$ feed. This is likely due to the higher Nafion loading on the GDE (218.5 μg $cm^{-2}$) compared to the H-cell electrode (87.4 μg $cm^{-2}$), and more importantly, the higher current density in MEA caused more reduction of sulfonic acid ($-SO_3H$) groups in the Nafion binder during $CO_2$ electrolysis. We can observe that the $Ag_2S$

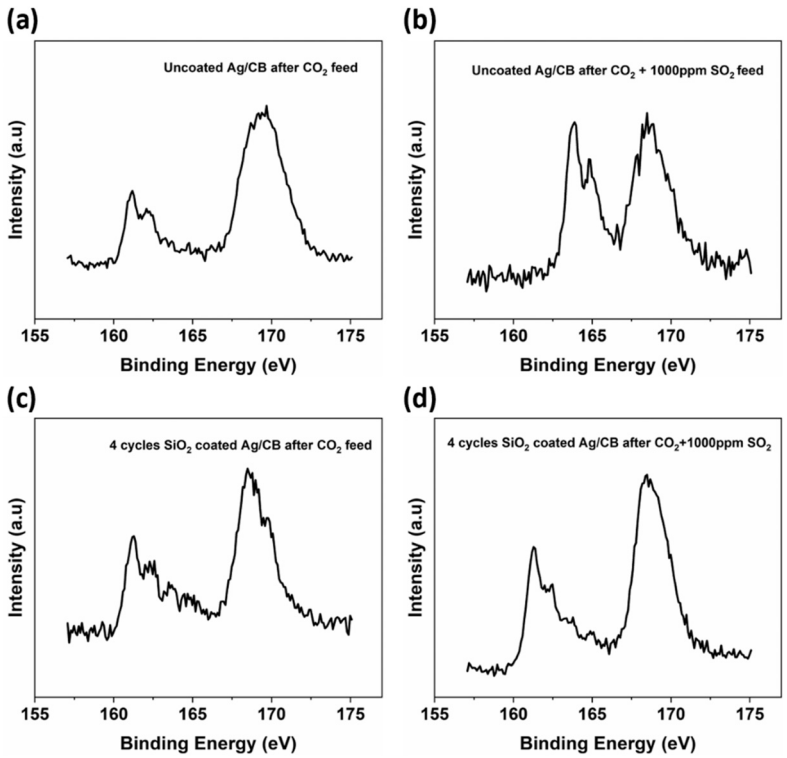


**Fig. 6** S 2p XPS spectrum of the Ag/CB catalyst after $CO_2$ electrolysis tested at MEA reactor at 100 mA $cm^{-2}$. (a) Ag/CB catalyst tested with $CO_2$ feed. (b) Ag/CB catalyst tested with $CO_2$ + 1000 ppm $SO_2$ feed. (c) Ag/CB catalyst with 4 cycles $SiO_2$ coating tested with $CO_2$ feed. (d) Ag/CB catalyst with 4 cycles $SiO_2$ coating tested with $CO_2$ + 1000 ppm $SO_2$ feed.

 

peak becomes stronger after shifting the feed gas from pure $CO_2$ to $CO_2$ combined with 1000 ppm $SO_2$ for the catalyst without $SiO_2$ coating. Nevertheless, for the catalyst coated with 4 cycles of $SiO_2$, the $Ag_2S$ peak remains almost identical with or without 1000 ppm $SO_2$ in the feed gas stream. This suggests that inhibition of $SO_2$ penetration by $SiO_2$ is also present in the MEA experiments.

$SO_2$ impurities in the $CO_2$ feed had a stronger influence on Ag/CB catalysts within the H-cell system than in the MEA reactor under the conditions used here. We attribute this difference in behaviour to the higher solubility of $SO_2$ in the liquid electrolyte compared to $CO_2$, resulting in an accumulation of $SO_2$ in the batchwise operated H-cell, but not in the MEA flow cell configuration. A visual representation of both cell geometries is provided in Fig. S7.† The solubility of $CO_2$ in water at 20 °C is 1.7 g $L^{-1}$. Under the same conditions, the solubility of $SO_2$ is 110 g $L^{-1}$, nearly 65 times higher than that of $CO_2$ in the electrolyte. This will lead to a continuous increase of $SO_2$ concentration in the electrolyte within the H-cell during the experiments until it reaches saturation. However, due to the high solubility of $SO_2$ in the electrolyte and the relatively low concentration of $SO_2$ in the feed gas stream, even with the highest concentration of $SO_2$ used in the experiments ($CO_2$ with 1000 ppm $SO_2$, which means 0.1 vol% of $SO_2$ in the $CO_2$ stream), it would require 6.6 days of continuous dosing to reach $SO_2$ saturation in the electrolyte. This implies that the electrolyte will never reach saturation during the H-cell experiments and the $SO_2$ concentration in the electrolyte will keep on increasing during the experiments. Consequently, the $SO_2$ concentration near the surface of the electrode will be much higher than in the feed gas for the H-cell experiments. On the contrary, in the MEA reactor geometry, the cathode is in direct contact with the feed gas, without the presence of electrolyte in the cathode serpentine channel. Therefore, the $SO_2$ concentration near the cathode in the MEA system is the same as in the feed gas, which is much lower than the concentration near the cathode in the H-cell system with the same feed gas composition. This explains why the Ag/CB catalyst in the MEA system is not significantly affected by $SO_2$ impurities and it shows that the Ag/CB catalyst can maintain its performance with 1000 ppm $SO_2$ impurities in the MEA system within our 25 minutes testing timeframe. The long-term stability of the Ag/CB catalyst in the MEA reactor under $SO_2$ impurities is worth investigating as well. However, after 50 minutes of CP testing, we encountered significant salt precipitation in the MEA system, resulting in a subsequent decrease in Faradaic efficiency. The first 18 minutes serve as a stabilization period, during which the reaction products are transferred to the GC. During this period, the Faradaic efficiency for both $H_2$ and CO is lower than expected. Additionally, the $FE_{CO}$ started to decrease after 35 minutes during CP testing with pure $CO_2$ gas feed at 100 mA $cm^{-2}$, as shown in Fig. S8.† Very obvious $KHCO_3$ salt precipitation can be seen on the cathode serpentine channel and gas diffusion electrode after 50 minutes CP testing (as shown in Fig. S9†). Nevertheless, the cell potential was relatively stable during 50 minutes CP testing, as can be seen in Fig. S10.† The minor fluctuation was due to the gas chromatography (GC) injection during the CP testing. Salt precipitation issues prevented us from further investigating the stability of Ag/CB catalyst in the MEA system, especially in the presence of $SO_2$ impurities. Therefore, this research question awaits further investigation in subsequent studies.

## Conclusions

We have explored the performance of the Ag/CB catalyst under $SO_2$ impurities for $CO_2$ electrolysis in two electrochemical cell geometries: an H-cell and a MEA cell. Both systems behave differently with respect to $SO_2$ contamination in the $CO_2$ feed. The impact of $SO_2$ on Ag/CB catalysts was large in the H-cell, while it was nearly absent in the MEA geometry under the relatively short testing time used in this study. This difference can be attributed to the greater solubility of $SO_2$ in the electrolyte compared to $CO_2$, leading to an accumulation effect and a much higher liquid phase concentration of $SO_2$ in the H-cell. This led to a greater performance decrease of the Ag/CB catalyst in the H-cell compared to the MEA geometry, when exposed to the same concentration of $SO_2$ impurities. An ultrathin $SiO_2$ coating synthesized *via* ALD protected the Ag/CB catalyst in the H-cell against $SO_2$ impurities under relatively less negative potentials. This is due to the $SO_2$ and $CO_2$ permeability differences through the $SiO_2$ coatings. $CO_2$ has much higher permeability compared to $SO_2$ (or $SO_2$ derived ions) through $SiO_2$. This leads to a significant obstruction in the interaction of $SO_2$ with the catalyst and might decrease the $SO_2$ concentration after the $SiO_2$ coatings.

## Data availability

The data supporting this article have been included as part of the ESI† see DOI: **https://doi.org/10.1039/D4CY01196A**.

## Author contributions

M. Li: conceptualization, methodology, formal analysis, validation, writing – original draft. S. Fu: methodology, validation, writing – review & editing. R. Kortlever: supervision, writing – review & editing, project administration. J. R. van Ommen: supervision, writing – review & editing, project administration, funding acquisition.

## Conflicts of interest

J. R. van Ommen has a financial interest in Powall.

## Acknowledgements

M. L. acknowledges the PhD scholarship awarded by the China Scholarship Council (CSC). The authors thank Saeed Saedy for doing the TG/DTA analysis, Cas Veenhoven for the

assistance in the lab, Bart Boshuizen for the XPS area scan training and Baukje Terpstra for the ICP-OES analysis.

## Notes and references

1 C. Chen, J. F. Khosrowabadi Kotyk and S. W. Sheehan, Progress toward Commercial Application of Electrochemical Carbon Dioxide Reduction, *Chem*, 2018, **4**(11), 2571–2586.
2 M. Ma, K. Liu, J. Shen, R. Kas and W. A. Smith, In Situ Fabrication and Reactivation of Highly Selective and Stable Ag Catalysts for Electrochemical $CO_2$ Conversion, *ACS Energy Lett.*, 2018, **3**(6), 1301–1306.
3 N. Zhang, X. Zhang, L. Tao, P. Jiang, C. Ye and R. Lin, *et al.* Silver Single-Atom Catalyst for Efficient Electrochemical $CO_2$ Reduction Synthesized from Thermal Transformation and Surface Reconstruction, *Angew. Chem., Int. Ed.*, 2021, **60**(11), 6170–6176.
4 H. Wang, Z. Han, L. Zhang, C. Cui, X. Zhu and X. Liu, *et al.* Enhanced CO selectivity and stability for electrocatalytic reduction of $CO_2$ on electrodeposited nanostructured porous Ag electrode, *J. CO2 Util.*, 2016, **15**, 41–49.
5 S.-Q. Liu, S.-W. Wu, M.-R. Gao, M.-S. Li, X.-Z. Fu and J.-L. Luo, Hollow Porous Ag Spherical Catalysts for Highly Efficient and Selective Electrocatalytic Reduction of $CO_2$ to CO, *ACS Sustainable Chem. Eng.*, 2019, **7**(17), 14443–14450.
6 J. Osiewacz, M. Löffelholz, L. Weseler and T. Turek, CO poisoning of silver gas diffusion electrodes in electrochemical $CO_2$ reduction, *Electrochim. Acta*, 2023, **445**, 142046.
7 D. E. Doronkin, T. S. Khan, T. Bligaard, S. Fogel, P. Gabrielsson and S. Dahl, Sulfur poisoning and regeneration of the Ag/$\gamma$-$Al_2O_3$ catalyst for $H_2$-assisted SCR of $NO_x$ by ammonia, *Appl. Catal., B*, 2012, **117–118**, 49–58.
8 F. Gobal and L. Majari Kasmaee, Polysulfide Poisoning of Ag Electrocatalyst during L-Ascorbate Ion Electro-oxidation in Alkaline Solution, *Chin. J. Catal.*, 2012, **33**(2–3), 267–274.
9 V. Houel, P. Millington, S. Pollington, S. Poulston, R. R. Rajaram and A. Tsolakis, Chemical deactivation of Ag/$Al_2O_3$ by sulphur for the selective reduction of $NO_x$ using hydrocarbons, *Catal. Today*, 2006, **114**(4), 334–339.
10 P. Bains, P. Psarras and J. Wilcox, $CO_2$ capture from the industry sector, *Prog. Energy Combust. Sci.*, 2017, **63**, 146–172.
11 T. Al-Attas, S. K. Nabil, A. S. Zeraati, H. S. Shiran, T. Alkayyali and M. Zargartalebi, *et al.* Permselective MOF-Based Gas Diffusion Electrode for Direct Conversion of $CO_2$ from Quasi Flue Gas, *ACS Energy Lett.*, 2022, **8**(1), 107–115.
12 G. Pipitone and O. Bolland, Power generation with $CO_2$ capture: Technology for $CO_2$ purification, *Int. J. Greenhouse Gas Control*, 2009, **3**(5), 528–534.
13 R. T. J. Porter, M. Fairweather, M. Pourkashanian and R. M. Woolley, The range and level of impurities in $CO_2$ streams from different carbon capture sources, *Int. J. Greenhouse Gas Control*, 2015, **36**, 161–174.
14 D. M. D'Alessandro, B. Smit and J. R. Long, Carbon dioxide capture: prospects for new materials, *Angew. Chem., Int. Ed.*, 2010, **49**(35), 6058–6082.
15 G. V. Last and M. T. Schmick, *Identification and Selection of Major Carbon Dioxide Stream Compositions*, US Department of Energy, 2011, PNNL-20493.
16 B. H. Ko, B. Hasa, H. Shin, E. Jeng, S. Overa and W. Chen, *et al.* The impact of nitrogen oxides on electrochemical carbon dioxide reduction, *Nat. Commun.*, 2020, **11**(1), 5856.
17 Y. Xu, J. P. Edwards, J. Zhong, C. P. O'Brien, C. M. Gabardo and C. McCallum, *et al.* Oxygen-tolerant electroproduction of C2 products from simulated flue gas, *Energy Environ. Sci.*, 2020, **13**(2), 554–561.
18 S. Van Daele, L. Hintjens, S. Hoekx, B. Bohlen, S. Neukermans and N. Daems, *et al.* How flue gas impurities affect the electrochemical reduction of $CO_2$ to CO and formate, *Appl. Catal., B*, 2024, **341**, 123345.
19 P. P. Albertini, M. A. Newton, M. Wang, O. Segura Lecina, P. B. Green and D. C. Stoian, *et al.* Hybrid oxide coatings generate stable Cu catalysts for $CO_2$ electroreduction, *Nat. Mater.*, 2024, **23**(5), 680–687.
20 H. Van Bui, F. Grillo and J. R. van Ommen, Atomic and molecular layer deposition: off the beaten track, *Chem. Commun.*, 2016, **53**(1), 45–71.
21 K. S. Yoo, D.-G. Kim, S. Lee, W.-B. Lee and J.-S. Park, Atmospheric pressure spatial ALD of $Al_2O_3$ thin films for flexible PEALD IGZO TFT application, *Ceram. Int.*, 2022, **48**(13), 18803–18810.
22 D. H. Levy, D. Freeman, S. F. Nelson, P. J. Cowdery-Corvan and L. M. Irving, Stable ZnO thin film transistors by fast open air atomic layer deposition, *Appl. Phys. Lett.*, 2008, **92**, 192101.
23 D. La Zara, F. Sun, F. Zhang, F. Franek, K. Balogh Sivars and J. Horndahl, *et al.* Controlled Pulmonary Delivery of Carrier-Free Budesonide Dry Powder by Atomic Layer Deposition, *ACS Nano*, 2021, **15**(4), 6684–6698.
24 J. W. Klaus and S. M. George, Atomic layer deposition of $SiO_2$ at room temperature using $NH_3$-catalyzed sequential surface reactions, *Surf. Sci.*, 1999, **447**(2000), 81–90.
25 F. Grillo, H. Van Bui, J. A. Moulijn, M. T. Kreutzer and J. R. van Ommen, Understanding and Controlling the Aggregative Growth of Platinum Nanoparticles in Atomic Layer Deposition: An Avenue to Size Selection, *J. Phys. Chem. Lett.*, 2017, **8**(5), 975–983.
26 M. Li, S. Fu, S. Saedy, A. Rajendrakumar, F. D. Tichelaar and R. Kortlever, *et al.* Nanostructuring Pt-Pd Bimetallic Electrocatalysts for $CO_2$ Reduction Using Atmospheric Pressure Atomic Layer Deposition, *ChemCatChem*, 2022, **14**, e202200949.
27 R. Kamphorst, P. Wanjari, S. Saedy, J. F. K. van Dam, A. Thijssen and P. Brüner, *et al.* Enhancing colloid stability of polymer microspheres in water through $SiO_2$ coating: Effects of coating cycles and surface coverage, *Surf. Interfaces*, 2024, **45**, 103852.
28 Y. Song and P. N. Pintauro, The electrochemical synthesis of aminonitriles I. H-cell studies with adiponitrile and azelanitrile, *J. Appl. Electrochem.*, 1991, **21**, 21–27.
29 L. Wang, C.-Y. Lee and P. Schmuki, Solar water splitting: preserving the beneficial small feature size in porous $\alpha$-$Fe_2O_3$ photoelectrodes during annealing, *J. Mater. Chem. A*, 2013, **1**(2), 212–215.

 

30 M. Li, S. Saedy, S. Fu, T. Stellema, R. Kortlever and J. R. van Ommen, Enhancing the durability of Pt nanoparticles for water electrolysis using ultrathin $SiO_2$ layers, *Catal. Sci. Technol.*, 2024, **14**(5), 1328–1335.

31 Y. Du, X. Du and S. M. George, SiO2 film growth at low temperatures by catalyzed atomic layer deposition in a viscous flow reactor, *Thin Solid Films*, 2005, **491**(1–2), 43–53.

32 J. W. Klaus, O. Sneh and S. M. George, Growth of $SiO_2$ at Room Temperature with the Use of Catalyzed Sequential Half-Reactions, *Science*, 1997, **278**(5345), 1934–1936.

33 H. Yun, J. Kim, W. Choi, M. H. Han, J. H. Park and H.-S. Oh, *et al.* Understanding morphological degradation of Ag nanoparticle during electrochemical $CO_2$ reduction reaction by identical location observation, *Electrochim. Acta*, 2021, **371**, 137795.

34 C. Kim, T. Eom, M. S. Jee, H. Jung, H. Kim and B. K. Min, *et al.* Insight into Electrochemical $CO_2$ Reduction on Surface-Molecule-Mediated Ag Nanoparticles, *ACS Catal.*, 2016, **7**(1), 779–785.

35 N. J. Harmon and H. Wang, Electrochemical $CO_2$ Reduction in the Presence of Impurities: Influences and Mitigation Strategies, *Angew. Chem., Int. Ed.*, 2022, **61**(52), e202213782.

36 S. Ghafoor, S. Ata, N. Mahmood and S. N. Arshad, Photosensitization of $TiO_2$ nanofibers by $Ag_2S$ with the synergistic effect of excess surface $Ti^{3+}$ states for enhanced photocatalytic activity under simulated sunlight, *Sci. Rep.*, 2017, **7**(1), 255.

37 F. M. Nor, N. H. A. Karim, I. Abdullah and R. Othaman, Permeability of carbon dioxide and nitrogen gases through $SiO_2$ and MgO incorporated ENR/PVC membranes, *J. Elastomers Plast.*, 2016, **48**(6), 483–498.

38 M. F. A. Wahab, A. F. Ismail and S. J. Shilton, Studies on gas permeation performance of asymmetric polysulfone hollow fiber mixed matrix membranes using nanosized fumed silica as fillers, *Sep. Purif. Technol.*, 2012, **86**, 41–48.

39 L. Meng, M. Kanezashi, J. Wang and T. Tsuru, Permeation properties of BTESE–TEOS organosilica membranes and application to $O_2/SO_2$ gas separation, *J. Membr. Sci.*, 2015, **496**, 211–218.

40 J. Yoshiura, K. Ishii, Y. Saito, T. Nagataki, Y. Nagataki and A. Ikeda, *et al.* Permeation Properties of Ions through Inorganic Silica-Based Membranes, *Membranes*, 2020, **10**, 27.

41 X. Yu, L. Meng, H. Nagasawa, M. Kanezashi, M. Machida and T. Tsuru, Evaluating the chemical stability of metal oxides in $SO_3$ and applications of $SiO_2$-based membranes to $O_2/SO_3$ separation, *J. Am. Ceram. Soc.*, 2019, **102**(11), 6946–6956.